IEEJ Journal of Industry Applications
Vol.8 No.2 pp.263–270 DOI: 10.1541/ieejjia.8.263

Paper

Perfect Tracking Control Considering Generalized Controllability Indices and Application for High-Precision Stage in Translation and Pitching

Masahiro Mae[*a)] Student Member, Wataru Ohnishi[*] Member
Hiroshi Fujimoto[*] Senior Member, Yoichi Hori[*] Fellow

(Manuscript received May 2, 2018, revised Sep. 28, 2018)

High-precision stages are widely used for manufacturing semiconductors and flat panels. These high-precision stages have become multi-input multi-output (MIMO) systems with six-degrees-of-freedom (DOF); hence, the coupling between the translation and pitching motion deteriorates the control performance. This study proposes the multirate feedforward control for MIMO systems and applies it to these high-precision stages. The multirate feedforward control designs the stable inversion for the unstable discretization zero problem. In addition, the design of the MIMO multirate feedforward controllers has a degree of freedom to design the $\boldsymbol{B}$ matrix according to the selection of the generalized controllability indices. In conventional control methods such as precompensated decoupling controllers, it is theoretically impossible to achieve perfect tracking because unstable discretization zeros are generated. In this study, the proposed method is applied to the translation and pitching motion of a high-precision stage, and it achieves perfect tracking in the simulation. The effectiveness of the proposed method is verified experimentally.

Keywords: multirate feedforward, multi-input multi-output system, high-precision stage

1. Introduction

A high-precision scan stage is critical in manufacturing semiconductors and flat panels [(1)]. The circuit configuration of semiconductors and flat panels becomes finer exponentially annually [(2)]. The conventional high-precision stage is a one-degree-of-freedom (DOF) system mechanically constrained to move only one direction. Recently, to decrease the disturbance of vibration from the floor and friction from the mechanical restraint, the high-precision stage is a six-DOF $(x, y, z, \theta_x, \theta_y, \theta_z)$ system by the gravity canceller that compensates for the gravitational force experienced by the fine stage [(1)]. In the stage with six-DOF, the interference forces between the axes worsen the positioning accuracy of the stage. Many studies have been conducted on the decoupling. The precompensator for decoupling is typically used to apply the single-input single-output (SISO) controllers to the coupled multi-input multi-output (MIMO) system [(1)]. The MIMO feedback controller and the integrated design of the mechanism and the controller are also used for decoupling, e.g., using the Direct Nyquist Array method and changing the height of the actuation point virtually [(3)].

From the viewpoint of designing the feedforward controller, the controller is designed in the continuous-time domain and discretized in the conventional method. In this approach, the controller cannot achieve perfect tracking control (PTC) theoretically because of the discretized unstable zeros. The word "perfect tracking control (PTC)" is defined as "the plant output perfectly tracks the desired trajectory with zero tracking error at every sampling point" [(4)]. In the proposed method, we use discretized plant models and design the controller in the discrete-time domain. Using this approach, PTC is achieved theoretically by considering the interference between axes using the MIMO multirate feedforward controller. The consideration of the input multiplicities in the digital control for the MIMO system is the important point.

In this study, the authors control a high-precision stage with six-DOF, as shown in Fig. 1(a). The authors consider two-DOF of translation in the x axis direction and pitching around the y axis, as shown in Fig. 1(b). The effectiveness of the proposed method is demonstrated by simulations and experiments.

a) Correspondence to: Masahiro Mae. E-mail: mmae@ieee.org
[*] The University of Tokyo
5-1-5, Kashiwanoha, Kashiwa, Chiba 227-8561, Japan

2. Proposed Method

2.1 Multirate Feedforward for Single-Input Single-Output System Multirate feedforward control achieves PTC [(6)]. A digital tracking control system typically has two samplers for the reference signal $r(t)$ and the output $y(t)$, and one holder on the input $u(t)$, as shown in Fig. 2. Therefore, three time periods exist: T_r, T_y, and T_u, representing the periods of $r(t)$, $y(t)$, and $u(t)$, respectively, as shown in Fig. 3. Additionally, the longer period of T_r or T_y is defined as the frame period T_f. In the case of the SISO nth-order plant, $T_r = nT_y = nT_u = T_f$.

Consider the continuous-time nth-order plant described by the state equation (1) and the output equation (2).

$$\dot{\boldsymbol{x}}(t) = \boldsymbol{A}_c\boldsymbol{x}(t) + \boldsymbol{b}_c u(t) \cdots\cdots (1)$$

$$y(t) = \boldsymbol{c}_c\boldsymbol{x}(t) \cdots\cdots (2)$$

From the discretization of (1) and (2) by the zero-order hold

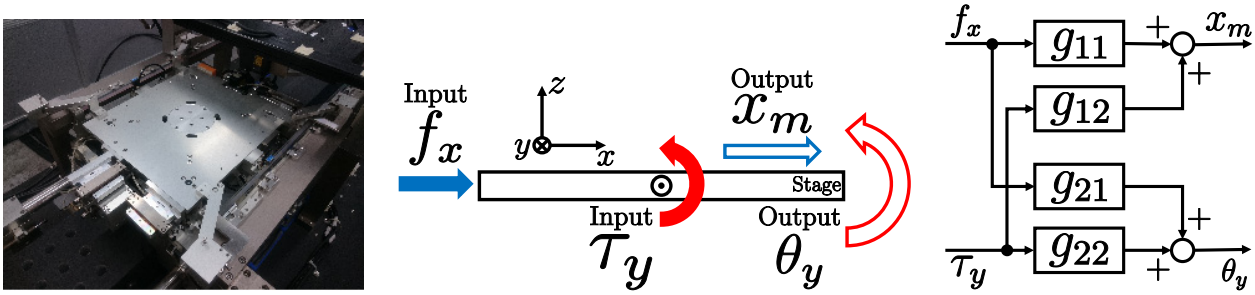

(a) Photograph of the six-DOF high-precision stage. (b) Coupling problem between x_m and θ_y. (c) Block diagram of the plant.

Fig. 1. Details of the plant

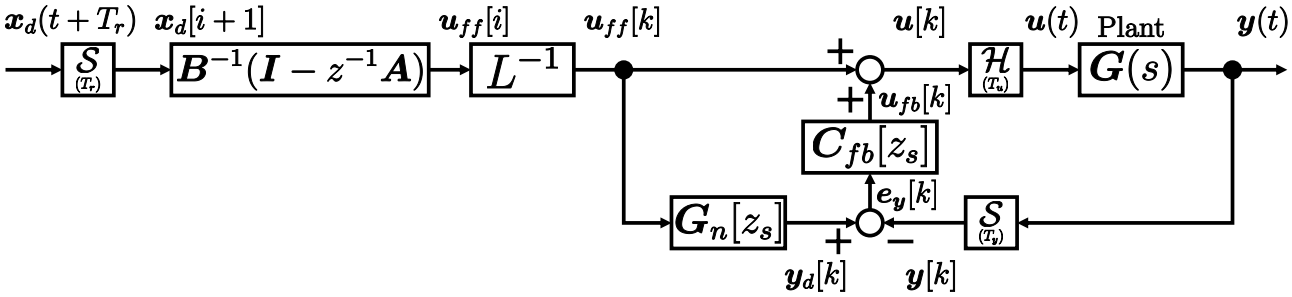

Fig. 2. Block diagram of the controller with the plant that does not contain unstable intrinsic zeros. $\mathcal{S}$, $\mathcal{H}$, and L denote a sampler, holder, and lifting operator [5], respectively; z and z_s denote e^{sT_r} and e^{sT_u}, respectively

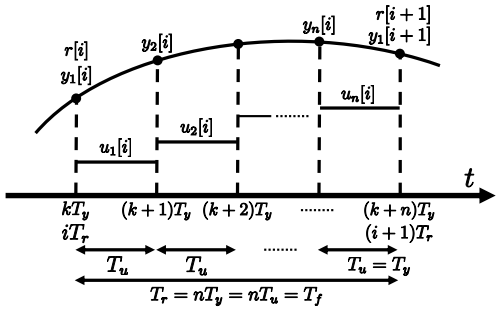

Fig. 3. SISO multirate sampling control at the same interval

in the sampling period T_u, the discrete-time plant becomes the state equation (3) and output equation (4).

$$\boldsymbol{x}[k+1] = \boldsymbol{A}_s\boldsymbol{x}[k] + \boldsymbol{b}_s u[k] \quad \cdots\cdots (3)$$

$$y[k] = \boldsymbol{c}_s\boldsymbol{x}[k] \quad \cdots\cdots (4)$$

where the matrices $\boldsymbol{A}_s$, $\boldsymbol{b}_s$, and $\boldsymbol{c}_s$ are given by

$$\boldsymbol{A}_s = e^{\boldsymbol{A}_c T_u}, \quad \boldsymbol{b}_s = \int_0^{T_u} e^{\boldsymbol{A}_c\tau}\boldsymbol{b}_c d\tau, \quad \boldsymbol{c}_s = \boldsymbol{c}_c.$$

By lifting the discrete-time state equation (3) and the output equation (4), the state equation (5) and the output equation (6) are given by

$$\boldsymbol{x}[i+1] = \boldsymbol{A}\boldsymbol{x}[i] + \boldsymbol{B}\boldsymbol{u}[i], \quad \cdots\cdots (5)$$

$$y[i] = \boldsymbol{c}\boldsymbol{x}[i], \quad \cdots\cdots (6)$$

where the matrices $\boldsymbol{A}$, $\boldsymbol{B}$, and $\boldsymbol{c}$, and i are given by

$$\boldsymbol{A} = \boldsymbol{A}_s^n, \quad \boldsymbol{B} = \begin{bmatrix}\boldsymbol{A}_s^{n-1}\boldsymbol{b}_s & \boldsymbol{A}_s^{n-2}\boldsymbol{b}_s & \cdots & \boldsymbol{A}_s\boldsymbol{b}_s & \boldsymbol{b}_s\end{bmatrix},$$
$$\boldsymbol{c} = \boldsymbol{c}_s, \quad \boldsymbol{x}[i] = \boldsymbol{x}(iT_r).$$

Equations (5) and (6) are given from the interval between $t = iT_r = kT_u$ and $t = (i+1)T_r = (k+n)T_u$. The input and output vectors $\boldsymbol{u}[i]$ (7) and $\boldsymbol{y}[i]$ (8) are given by

$$\begin{aligned}\boldsymbol{u}[i] &= \begin{bmatrix}u_1[i] & u_2[i] & \cdots & u_n[i]\end{bmatrix}^{\mathsf{T}} \\ &= \begin{bmatrix}u(kT_u) & u((k+1)T_u) & \cdots & u((k+n-1)T_u)\end{bmatrix}^{\mathsf{T}}, \quad \cdots\cdots (7)\end{aligned}$$

$$\begin{aligned}\boldsymbol{y}[i] &= \begin{bmatrix}y_1[i] & y_2[i] & \cdots & y_n[i]\end{bmatrix}^{\mathsf{T}} \\ &= \begin{bmatrix}y(kT_y) & y((k+1)T_y) & \cdots & y((k+n-1)T_y)\end{bmatrix}^{\mathsf{T}}. \quad \cdots\cdots (8)\end{aligned}$$

From (5), the control input $\boldsymbol{u}_{ff}[i]$ to achieve PTC are given by

$$\boldsymbol{u}_{ff}[i] = \boldsymbol{B}^{-1}(\boldsymbol{I} - z^{-1}\boldsymbol{A})\boldsymbol{x}[i+1]. \quad \cdots\cdots (9)$$

The block diagram of the control system is shown in Fig. 2. L is a discrete-time lifting operator [5]. L^{-1} outputs the elements of the nth dimensional vector $\boldsymbol{u}_{ff}[i]$, which is input at every period T_r, in the order from 1 to n by $T_u = T_r/n$.

2.2 Multirate Feedforward for Multi-Input Multi-Output System In an m-input p-output nth order MIMO system, the state equation (10) and the output equation (11) of the continuous-time plant are given by

$$\dot{\boldsymbol{x}}(t) = \boldsymbol{A}_c\boldsymbol{x}(t) + \boldsymbol{B}_c\boldsymbol{u}(t), \quad \cdots\cdots (10)$$

$$\boldsymbol{y}(t) = \boldsymbol{C}_c\boldsymbol{x}(t), \quad \cdots\cdots (11)$$

$$\boldsymbol{B}_c = \begin{bmatrix}\boldsymbol{b}_{c1} & \cdots & \boldsymbol{b}_{cm}\end{bmatrix}, \quad \boldsymbol{C}_c = \begin{bmatrix}\boldsymbol{c}_{c1} & \cdots & \boldsymbol{c}_{cp}\end{bmatrix}^{\mathsf{T}},$$

where the plant state is $\boldsymbol{x} \in \mathbb{R}^n$, the plant input is $\boldsymbol{u} \in \mathbb{R}^m$, and the plant output is $\boldsymbol{u} \in \mathbb{R}^p$.

The generalized controllability indices are defined as follows [7]:

Definition (Generalized Controllability Indices). *The generalized controllability indices of $(\boldsymbol{A}_c, \boldsymbol{B}_c)$ are defined as follows for $\boldsymbol{A}_c \in \mathbb{R}^{n\times n}$ and $\boldsymbol{B}_c = [\boldsymbol{b}_{c1}, \cdots, \boldsymbol{b}_{cm}] \in \mathbb{R}^{n\times m}$, respectively. If $(\boldsymbol{A}_c, \boldsymbol{B}_c)$ is a controllable pair, n linearly independent vectors including the linear combination can be selected*

from $\{\boldsymbol{b}_{c1}, \cdots, \boldsymbol{b}_{cm}, \boldsymbol{A}_c\boldsymbol{b}_{c1}, \cdots, \boldsymbol{A}_c\boldsymbol{b}_{cm}, \cdots, \boldsymbol{A}_c^{n-1}\boldsymbol{b}_{cm}\}$.

Setting φ as a set of these n vectors, σ_l and N are defined by

$$\sigma_l = \text{number}\{k|\boldsymbol{A}_c^{k-1}\boldsymbol{b}_{cl} \in \varphi\}, \cdots\cdots\cdots\cdots\cdots (12)$$

$$\sum_{l=1}^{m} \sigma_l = n, \cdots\cdots\cdots\cdots\cdots\cdots\cdots\cdots\cdots (13)$$

$$N = \max(\sigma_l). \cdots\cdots\cdots\cdots\cdots\cdots\cdots\cdots\cdots (14)$$

In the MIMO system, n (= plant order) number of vectors are selected from the generalized controllability indices, and the full row rank matrix $\boldsymbol{B}$ are designed for almost all sampling period of the discretization†. Therefore, the feedforward controllers designed according to their different forms.

From (15), the control input $\boldsymbol{u}_{ff}[i]$ to achieve PTC are given by (16).

$$\boldsymbol{x}[i+1] = \boldsymbol{A}\boldsymbol{x}[i] + \boldsymbol{B}\boldsymbol{u}[i], \cdots\cdots\cdots\cdots\cdots\cdots (15)$$

$$\boldsymbol{u}_{ff}[i] = \boldsymbol{B}^{-1}(\boldsymbol{I} - z^{-1}\boldsymbol{A})\boldsymbol{x}[i+1], \cdots\cdots\cdots\cdots (16)$$

where the matrices $\boldsymbol{A}$, $\boldsymbol{x}[i]$, $\boldsymbol{u}[i]$, z and T_f are given by

$$\boldsymbol{A} = e^{\boldsymbol{A}_c T_f}, \quad \boldsymbol{x}[i] = \boldsymbol{x}(iT_f), \quad z = e^{sT_f}, \quad T_f = NT_u,$$

$$\boldsymbol{u}[i] = \begin{bmatrix}\boldsymbol{u}_1[i] & \cdots & \boldsymbol{u}_m[i]\end{bmatrix}^{\mathsf{T}}$$

$$= \begin{bmatrix}u_{11}[i] & \cdots & u_{1\sigma_1}[i] & u_{21}[i] & \cdots & u_{m\sigma_m}[i]\end{bmatrix}^{\mathsf{T}}.$$

3. Modeling

In the simulation and experiment, the authors controlled the fine stage of the six-DOF high-precision stage shown in Fig. 1(a). This fine stage is supported by a six-DOF air bearing gravity canceller. In this study, the two-DOF of the translation x along the x axis and the pitching θ_y around the y axis are controlled, as shown in Fig. 1(b).

3.1 System Identification The equations of motion of the translation and pitching of the stage are given by (17) and (18) [8].

$$(M_{x1} + M_{x2})\ddot{x}_{g1} + C_{x1}\dot{x}_{g1} + K_{x1}x_{g1} + M_{x2}L_{g2}\ddot{\theta}_y = f_x \cdots (17)$$

$$(M_{x2}L_{g2}^2 + J_{\theta y})\ddot{\theta}_y + C_{\theta y}\dot{\theta}_y + K_{\theta y}\theta_y + M_{x2}L_{g2}(\ddot{x}_{g1} - g\theta_y) = \tau_y + f_x L_{fx} \cdots (18)$$

Convert x_{g1} to observable x_m by (19).

$$x_m(s) = x_{g1}(s) + L_m\theta_y(s) \cdots\cdots\cdots\cdots\cdots\cdots (19)$$

From the expressions (17), (18), and (19), the transfer functions g_{11} to g_{22} are given by (20) to (23).

The parameters of the stage are shown in Table 1, which is given from fitting in the frequency domain, shown in Fig. 6.

3.2 State Space Realization a_{ij}, b_{ik} ($i \in \{2,4\}$, $j \in \{1,2,3,4\}$, $k \in \{1,2\}$) from the expressions (17), (18), and (19), $(\ddot{x}_m, \ddot{\theta}_y)$ explained by $(x_m, \dot{x}_m, \theta_y, \dot{\theta}_y)$ are given by (25) and (26).

$$\ddot{x}_m = a_{21}x_m + a_{22}\dot{x}_m + a_{23}\theta_y + a_{24}\dot{\theta}_y + b_{21}f_x + b_{22}\tau_y \cdots (25)$$

$$\ddot{\theta}_y = a_{41}x_m + a_{42}\dot{x}_m + a_{43}\theta_y + a_{44}\dot{\theta}_y + b_{41}f_x + b_{42}\tau_y \cdots (26)$$

† This is possible because the controllability of the continuous-time system is not preserved in the discrete system only if the two poles η_i and η_j have the same real parts, and the discretizing sampling period T satisfies $\eta_i = \eta_j + j\frac{2k\pi}{T}$ ($k = \pm1, \pm2, \ldots$); further, it is limited to only several cases.

Table 1. Model parameters

Symbol	Meaning	Value
x_m	Measured position of the fine stage	–
x_{g1}	Position of the CoG of the planar air bearing and the air gyro	–
x_{g2}	Position of the CoG of the fine stage	–
θ_y	Measured attitude angle of the fine stage	–
f_x	Input force of the fine stage in the x direction	–
τ_y	Input torque of the fine stage in the θ_y direction	–
M_{x1}	Mass of the planar air bearing and the air gyro	0.077 kg
C_{x1}	Viscosity coefficient in the x_{g1} motion	300 N/(m/s)
K_{x1}	Spring coefficient in the x_{g1} motion	6000 N/m
M_{x2}	Mass of the fine stage	5.3 kg
$J_{\theta y}$	Moment of inertia of the fine stage	0.10 kgm^2
$C_{\theta y}$	Viscosity coefficient of the fine stage in the θ_y motion	1.6 Nm/(rad/s)
$K_{\theta y}$	Spring coefficient of the fine stage in the θ_y motion	1200 Nm/rad
L_m	Distance between the measurement point of x_m and the CoR	−0.028 m
L_{g2}	Distance between the CoR and the CoG of the fine stage	−0.051 m
L_{fx}	Distance between the CoR of the fine stage and the actuation point	−0.0026 m

The state equations (27) and output equations (28) of the continuous-time plant are given by

$$\dot{\boldsymbol{x}}(t) = \boldsymbol{A}_c\boldsymbol{x}(t) + \boldsymbol{B}_c\boldsymbol{u}(t), \cdots\cdots\cdots\cdots\cdots (27)$$

$$\boldsymbol{y}(t) = \boldsymbol{C}_c\boldsymbol{x}(t), \cdots\cdots\cdots\cdots\cdots\cdots\cdots (28)$$

where the vectors $\boldsymbol{x}(t)$, $\boldsymbol{u}(t)$, and $\boldsymbol{y}(t)$, and the matrices $\boldsymbol{A}_c$, $\boldsymbol{B}_c$, and $\boldsymbol{C}_c$ are given by

$$\boldsymbol{x}(t) = \begin{bmatrix}x_m \\ \dot{x}_m \\ \theta_y \\ \dot{\theta}_y\end{bmatrix}, \quad \boldsymbol{u}(t) = \begin{bmatrix}f_x \\ \tau_y\end{bmatrix}, \quad \boldsymbol{y}(t) = \begin{bmatrix}x_m \\ \theta_y\end{bmatrix},$$

$$\boldsymbol{A}_c = \begin{bmatrix}0 & 1 & 0 & 0 \\ a_{21} & a_{22} & a_{23} & a_{24} \\ 0 & 0 & 0 & 1 \\ a_{41} & a_{42} & a_{43} & a_{44}\end{bmatrix}, \quad \boldsymbol{C}_c = \begin{bmatrix}1 & 0 & 0 & 0 \\ 0 & 0 & 1 & 0\end{bmatrix},$$

$$\boldsymbol{B}_c = \begin{bmatrix}0 & 0 \\ b_{21} & b_{22} \\ 0 & 0 \\ b_{41} & b_{42}\end{bmatrix} = \begin{bmatrix}\boldsymbol{b}_{c1} & \boldsymbol{b}_{c2}\end{bmatrix}.$$

By using the zero-order hold in the state equation (27) and the output equation (28) of the continuous-time plant with the sampling period T_u, the state equation (29) and the output equation (30) of the discrete-time plant are given by

$$\boldsymbol{x}[k+1] = \boldsymbol{A}_s\boldsymbol{x}[k] + \boldsymbol{B}_s\boldsymbol{u}[k], \cdots\cdots\cdots\cdots\cdots (29)$$

$$\boldsymbol{y}[k] = \boldsymbol{C}_s\boldsymbol{x}[k], \cdots\cdots\cdots\cdots\cdots\cdots\cdots (30)$$

where $\boldsymbol{x}[k]$, $\boldsymbol{u}[k]$, $\boldsymbol{y}[k]$, and $\boldsymbol{B}_s$ are given by

$$\boldsymbol{x}[k] = \begin{bmatrix}x_m[k] \\ \dot{x}_m[k] \\ \theta_y[k] \\ \dot{\theta}_y[k]\end{bmatrix}, \quad \boldsymbol{u}[k] = \begin{bmatrix}f_x[k] \\ \tau_y[k]\end{bmatrix}, \quad \boldsymbol{y}[k] = \begin{bmatrix}x_m[k] \\ \theta_y[k]\end{bmatrix},$$

$$\boldsymbol{B}_s = \begin{bmatrix}\boldsymbol{b}_{s1} & \boldsymbol{b}_{s2}\end{bmatrix}.$$

When constructing the square matrix $\boldsymbol{B}$, the generalized controllability indices are given by

$$\{\boldsymbol{b}_{s1}, \boldsymbol{b}_{s2}, \boldsymbol{A}_s\boldsymbol{b}_{s1}, \boldsymbol{A}_s\boldsymbol{b}_{s2}, \boldsymbol{A}_s^2\boldsymbol{b}_{s1}, \boldsymbol{A}_s^2\boldsymbol{b}_{s2}, \boldsymbol{A}_s^3\boldsymbol{b}_{s1}, \boldsymbol{A}_s^3\boldsymbol{b}_{s2}\}.$$

When the plant order is $n = 4$, four elements are chosen from the generalized controllability indices to construct the square matrix $\boldsymbol{B}$.

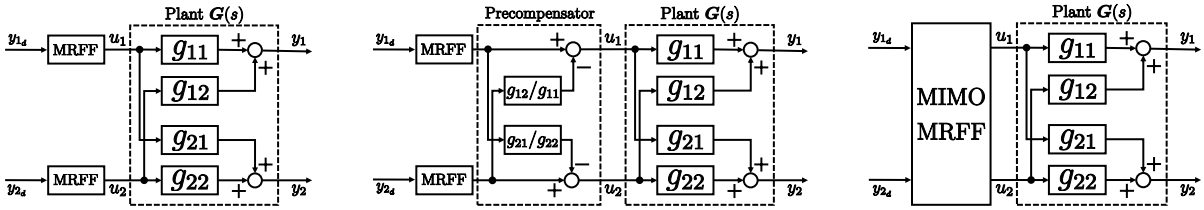

(a) Conventional method 1. (b) Conventional method 2. (c) Proposed method.

Fig. 4. Block diagram of the control methods. These show only feedforward controllers

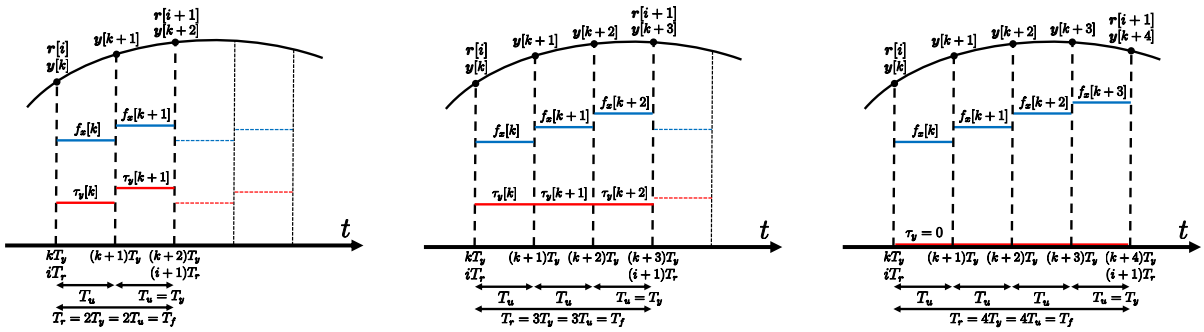

(a) $(\sigma_1, \sigma_2) = (2, 2)$ (b) $(\sigma_1, \sigma_2) = (3, 1)$ (c) $(\sigma_1, \sigma_2) = (4, 0)$

Fig. 5. MIMO multirate sampling control at the same interval

$$g_{11}(s)=\frac{x_m(s)}{f_x(s)} = \frac{[J_{\theta y}+L_{fx}L_mM_{x1}-(L_{fx}-L_{g2})(L_{g2}-L_m)M_{x2}]s^2+(C_{\theta y}+L_{fx}L_mC_{x1})s+L_{fx}L_mK_{x1}-L_{g2}M_{x2}g}{D(s)} \quad \cdots\cdots (20)$$

$$g_{12}(s)=\frac{x_m(s)}{\tau_y(s)} = \frac{[L_mM_{x1}+(L_m-L_{g2})M_{x2}]s^2+L_mC_{x1}s+L_mK_{x1}}{D(s)} \quad \cdots\cdots (21)$$

$$g_{21}(s)=\frac{\theta_y(s)}{f_x(s)} = \frac{[L_{fx}M_{x1}+(L_{fx}-L_{g2})M_{x2}]s^2+L_{fx}C_{x1}s+L_{fx}K_{x1}}{D(s)} \quad \cdots\cdots (22)$$

$$g_{22}(s)=\frac{\theta_y(s)}{\tau_y(s)} = \frac{(M_{x1}+M_{x2})s^2+C_{x1}s+K_{x1}}{D(s)} \quad \cdots\cdots (23)$$

$$D(s)=[(M_{x1}+M_{x2})J_{\theta y}+M_{x1}M_{x2}L_{g2}^2]s^4+[(M_{x1}+M_{x2})C_{\theta y}+(J_{\theta y}+M_{x2}L_{g2}^2)C_{x1}]s^3$$
$$+[(J_{\theta y}+M_{x2}L_{g2}^2)K_{x1}+(M_{x1}+M_{x2})(K_{\theta y}-M_{x2}L_{g2}g)+C_{\theta y}C_{x1}]s^2+[C_{\theta y}K_{x1}+C_{x1}(K_{\theta y}-L_{g2}M_{x2}g)]s+K_{x1}(K_{\theta y}-L_{g2}M_{x2}g) \quad \cdots\cdots (24)$$

4. Experiment

4.1 Condition The block diagram of the simulation is shown in Fig. 2. Generally, a dual-input dual-output plant with a coupling problem is represented by a block diagram, as shown in Fig. 1(c). g_{11} to g_{22} represent the transfer function of each path. Conventional method 1 ignores the interference by g_{12} and g_{21} and the multirate feedforward controllers are designed for each SISO system g_{11} and g_{22}, respectively, as shown in Fig. 4(a). Coupling is suppressed by the feedback controller. Conventional method 2 designs a precompensator for continuous-time plants that cancels the interference between axes by g_{12} and g_{21}, and the multirate feedforward controllers are designed for each decoupled SISO system g_{11} and g_{22}, respectively, as shown in Fig. 4(b). In this method, the precompensator is discretized by the bilinear transformation. Because the problem of the unstable discretization zero is not considered, PTC cannot be achieved, theoretically. In the proposed method, a dual-input dual-output multirate feedforward controller is designed for a dual-input dual-output plant, as shown in Fig. 4(c).

In Fig. 6, $\boldsymbol{G}_4$ is used for the MIMO plant model of the proposed method, and $\boldsymbol{G}_2$ is used for the SISO plant model of the conventional methods 1 and 2. The nominal plant g_{12} and g_{21} contain some gaps with the frequency response data because these four transfer functions, g_{11} to g_{22}, are correlated in this system and a trade off exists in the fitting. In this model, we focus on the fitting of the transfer function g_{21} representing the coupling from the translational force f_x along the x axis to the rotation θ_y around the y axis to prevent pitching.

In the simulation, $\boldsymbol{C}_{fb}[z_s]$, which is the feedback controller, is 0 in all the methods. In the experiment, $\boldsymbol{C}_{fb}[z_s]$ is a PID controller designed as 20 Hz closed-loop pole for all six-DOF $(x, y, z, \theta_x, \theta_y, \theta_z)$ in all the methods.

The seventh-order polynomial trajectory of 0 μm to 100 μm in 0 ms to 20 ms is given for x_m^{ref}, and a zero constant reference is given for θ_y^{ref}. $T_u = 200\,\mu$s, $N = \max(\sigma_1, \sigma_2)$, and $T_r = NT_y = NT_u = T_f$.

4.2 Simulation Result In this study, the simulation of the proposed method, in which the generalized controllability indices can be selected in three ways, as shown in Fig. 5, is conducted with the conventional method.

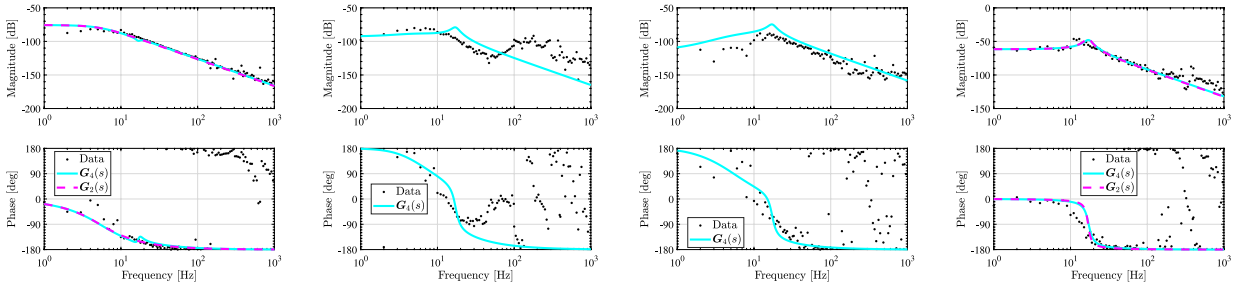

(a) g_{11} (b) g_{12} (c) g_{21} (d) g_{22}

Fig. 6. Frequency responses of the plant. $\boldsymbol{G}_4$ and $\boldsymbol{G}_2$ denote a 4th order MIMO nominal plant and a 2nd order SISO nominal plant, respectively

$$(\sigma_1,\sigma_2)=(2,2):\boldsymbol{B}=\begin{bmatrix}\boldsymbol{A}_s\boldsymbol{b}_{s1} & \boldsymbol{b}_{s1} & \boldsymbol{A}_s\boldsymbol{b}_{s2} & \boldsymbol{b}_{s2}\end{bmatrix} \quad \cdots\cdots (31)$$

$$(\sigma_1,\sigma_2)=(3,1):\boldsymbol{B}=\begin{bmatrix}\boldsymbol{A}_s^2\boldsymbol{b}_{s1} & \boldsymbol{A}_s\boldsymbol{b}_{s1} & \boldsymbol{b}_{s1} & \boldsymbol{A}_s^2\boldsymbol{b}_{s2}+\boldsymbol{A}_s\boldsymbol{b}_{s2}+\boldsymbol{b}_{s2}\end{bmatrix} \quad \cdots\cdots (32)$$

$$(\sigma_1,\sigma_2)=(4,0):\boldsymbol{B}=\begin{bmatrix}\boldsymbol{A}_s^3\boldsymbol{b}_{s1} & \boldsymbol{A}_s^2\boldsymbol{b}_{s1} & \boldsymbol{A}_s\boldsymbol{b}_{s1} & \boldsymbol{b}_{s1}\end{bmatrix} \quad \cdots\cdots (33)$$

The simulation result is shown in Fig. 7 to Fig. 11. Fig. 12 and Fig. 13 show the tracking error of each output. From the simulation results, PTC cannot be achieved with the conventional method, but it can be achieved in all three cases of the proposed method. The effectiveness of the proposed method is verified. It is noteworthy that the second-order relative degree plant moves the second-order polynomial trajectory between the sampling points. Therefore, the errors occur between the sampling points because of the difference in the order between the second-order polynomial trajectory and the seventh-order polynomial trajectory. This is an error because of the physical model, and not a mechanical vibration.

4.3 Experimental Results In the experiment, the proposed method of $(\sigma_1,\sigma_2)=(2,2)$, conventional method 1, and conventional method 2 are compared under the same conditions as the simulation.

The experimental result is shown in Fig. 14. From the experimental results, the tracking error of θ_y in the proposed method is the smallest compared with that in the conventional methods. The tracking error of x_m in the proposed method is not clearly smaller than that of other conventional methods, because we focus on the fitting of the transfer function g_{21} representing the coupling from the translational force f_x along the x axis to the rotation θ_y around the y axis to prevent pitching in this model. Therefore, the modeling error of g_{12} may worse the tracking error of x_m. The coupling of the feedback controllers is also a problem. Because it is verified that the tracking error becomes smaller and the control performance improves in the simulation that has no modeling error, it appears that the modeling error influences the experiment. From the simulation and experimental results, the applicability of the proposed method is verified and the improvement in the modeling error will be future work.

5. Conclusion

The six-DOF high-precision stage has the coupling problem. In the conventional methods, decoupling methods such as using a precompensator have been employed, and the system was controlled as a SISO system. However, when the precompensator and SISO multirate feedforward controller were used, it was theoretically impossible to achieve PTC because the unstable zeros were generated by discretization. In the proposed method, the MIMO multirate feedforward controller achieved PTC. In this study, the effectiveness of the proposed method was shown in the simulation and experiment of controlling two-DOF (x,θ_y) of the high-precision stage. The differences in the control performance depending on the selection of the generalized controllability indices will be considered in future studies. The proposed method loosened the restrictions of the mechanical design to suppress the coupling problem; therefore, the freedom of the mechanical design was improved.

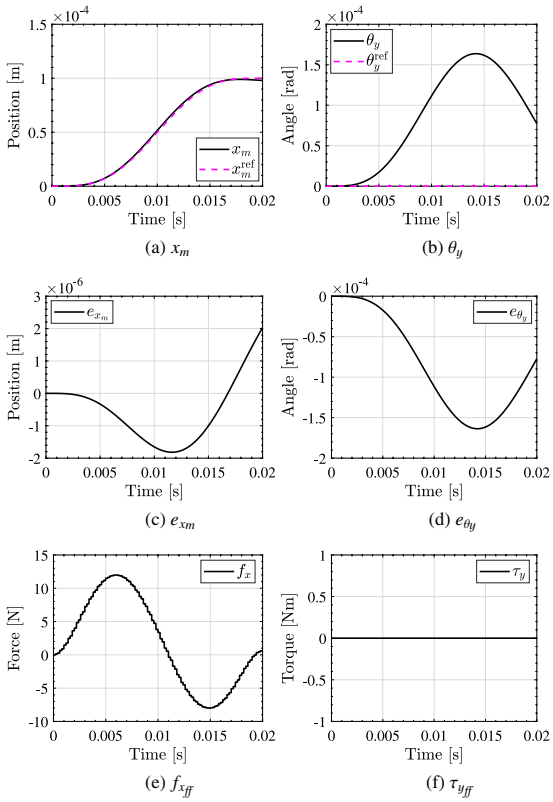

(a) x_m (b) θ_y (c) e_{xm} (d) $e_{\theta y}$ (e) $f_{x_{ff}}$ (f) $\tau_{y_{ff}}$

Fig. 7. Simulation results of the conventional method 1

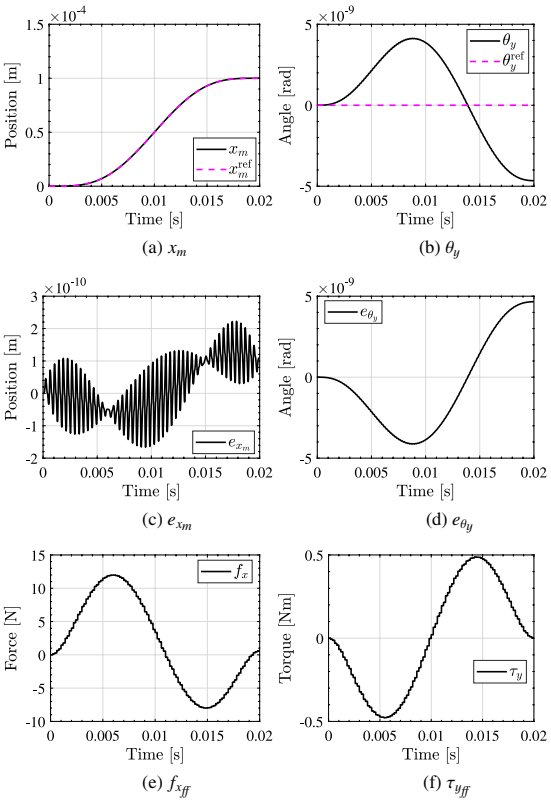

(a) x_m (b) θ_y (c) e_{xm} (d) $e_{\theta y}$ (e) $f_{x_{ff}}$ (f) $\tau_{y_{ff}}$

Fig. 8. Simulation results of the conventional method 2

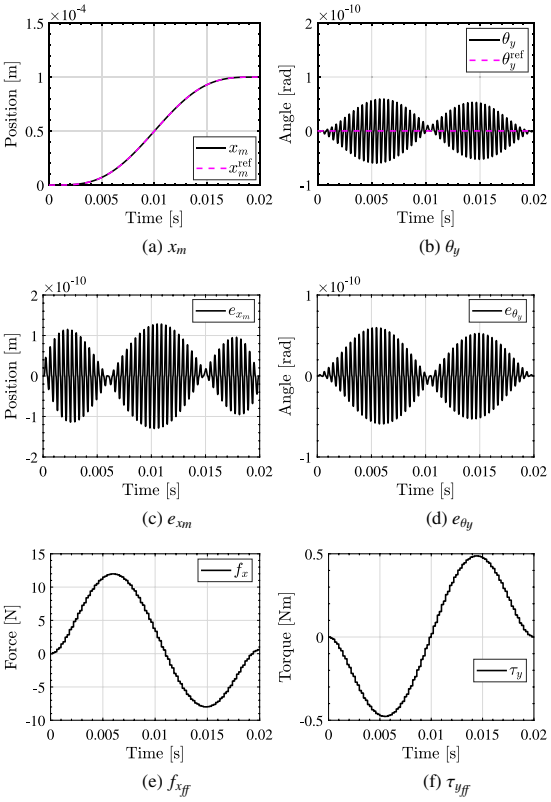

(a) x_m (b) θ_y (c) e_{xm} (d) $e_{\theta y}$ (e) $f_{x_{ff}}$ (f) $\tau_{y_{ff}}$

Fig. 9. Simulation results of the proposed method $(\sigma_1, \sigma_2) = (2, 2)$

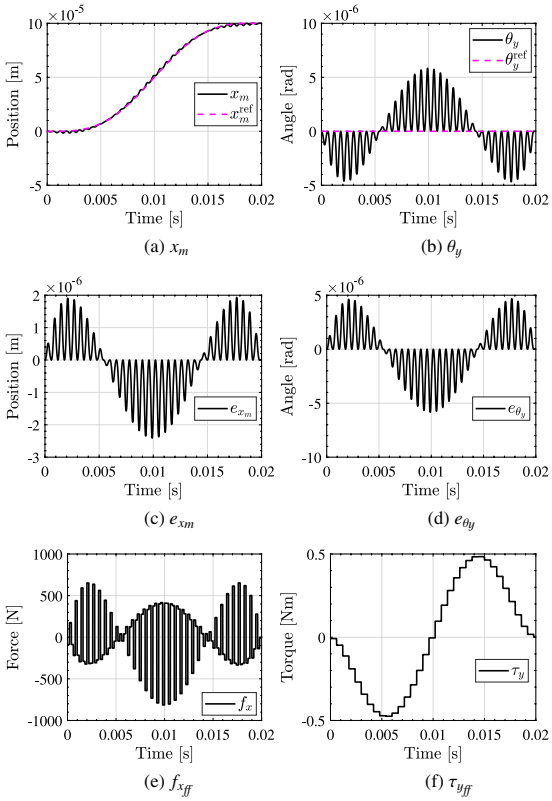

(a) x_m (b) θ_y (c) e_{xm} (d) $e_{\theta y}$ (e) $f_{x_{ff}}$ (f) $\tau_{y_{ff}}$

Fig. 10. Simulation results of the proposed method $(\sigma_1, \sigma_2) = (3, 1)$

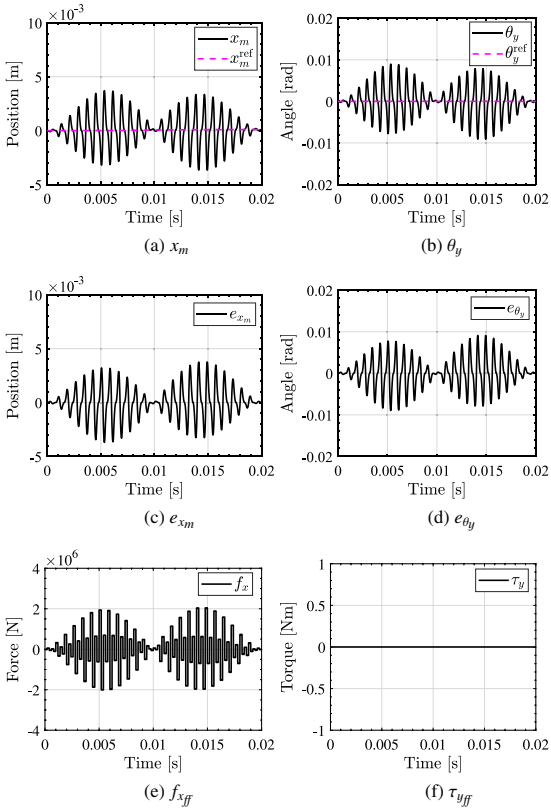

(a) x_m (b) θ_y (c) e_{xm} (d) $e_{\theta y}$ (e) $f_{x_{ff}}$ (f) $\tau_{y_{ff}}$

Fig. 11. Simulation results of the proposed method $(\sigma_1, \sigma_2) = (4, 0)$

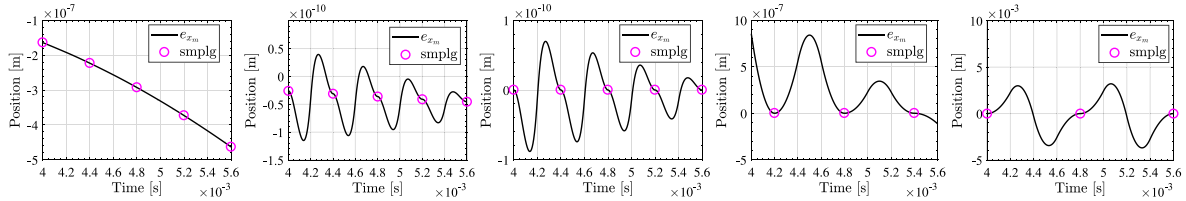

(a) Conventional method 1. (b) Conventional method 2. (c) Proposed method $(\sigma_1, \sigma_2) = (2, 2)$. (d) Proposed method $(\sigma_1, \sigma_2) = (3, 1)$. (e) Proposed method $(\sigma_1, \sigma_2) = (4, 0)$.

Fig. 12. Simulation result of e_{x_m} (zoom)

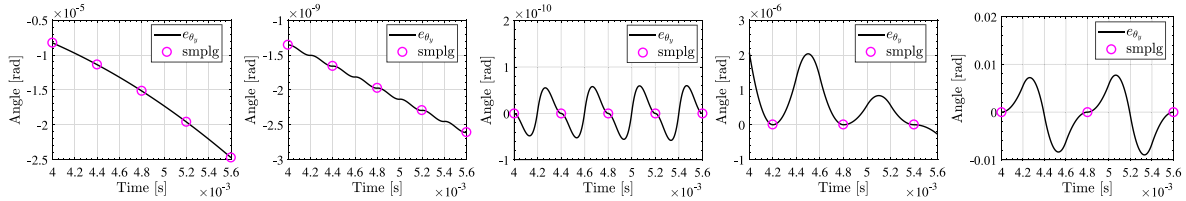

(a) Conventional method 1. (b) Conventional method 2. (c) Proposed method $(\sigma_1, \sigma_2) = (2, 2)$. (d) Proposed method $(\sigma_1, \sigma_2) = (3, 1)$. (e) Proposed method $(\sigma_1, \sigma_2) = (4, 0)$.

Fig. 13. Simulation result of e_{θ_y} (zoom)

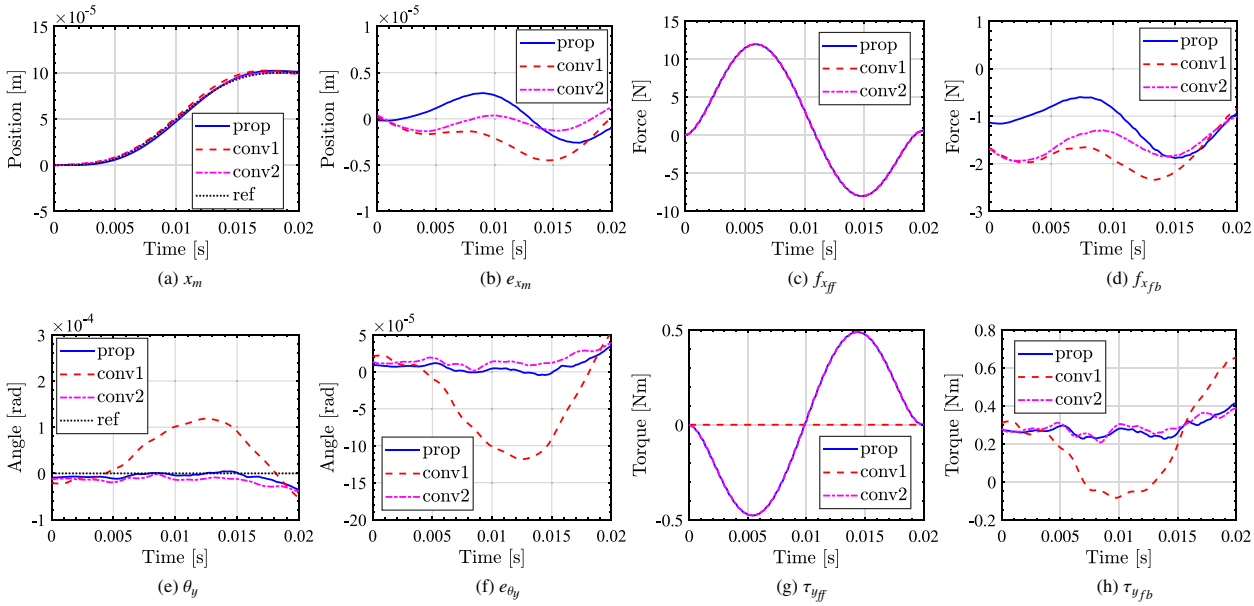

(a) x_m (b) e_{x_m} (c) $f_{x_{ff}}$ (d) $f_{x_{fb}}$

(e) θ_y (f) e_{θ_y} (g) $\tau_{y_{ff}}$ (h) $\tau_{y_{fb}}$

Fig. 14. Experimental results

References

(1) H. Butler: "Position Control in Lithographic Equipment", *IEEE Control Systems*, Vol.31, No.5, pp.28–47 (2011)

(2) G.E. Moore: "Cramming More Components Onto Integrated Circuits", *Electronics*, Vol.38, No.8 (1965)

(3) W. Ohnishi, H. Fujimoto, K. Sakata, K. Suzuki, and K. Saiki: "Integrated design of mechanism and control for high-precision stages by the interaction index in the Direct Nyquist Array method", in American Control Conference, pp.2825–2830 (2015)

(4) M. Tomizuka: "Zero Phase Error Tracking Algorithm for Digital Control", *Journal of Dynamic Systems, Measurement, and Control*, Vol.109, No.1, p.65 (1987)

(5) T. Chen and B.A. Francis: Optimal Sampled-Data Control Systems, Springer London, London (1995)

(6) H. Fujimoto, Y. Hori, and A. Kawamura: "Perfect tracking control based on multirate feedforward control with generalized sampling periods", *IEEE Transactions on Industrial Electronics*, Vol.48, No.3, pp.636–644 (2001)

(7) H. Fujimoto: General Framework of Multirate Sampling Control and Applications to Motion Control Systems, PhD thesis (2000)

(8) W. Ohnishi, H. Fujimoto, K. Sakata, K. Suzuki, and K. Saiki: "Decoupling Control Method for High-Precision Stages using Multiple Actuators considering the Misalignment among the Actuation Point, Center of Gravity, and Center of Rotation", *IEEJ Journal of Industry Applications*, Vol.5, No.2, pp.141–147 (2016)

Masahiro Mae (Student Member) received the B.E. degree from the University of Tokyo, Japan in 2018. He is currently working towards the M.S. degree in the Department of Advanced Energy, Graduate School of Frontier Sciences, the University of Tokyo. His interests are in control engineering, motion control, and nanoscale servo systems. He is a student member of the Institute of Electrical and Electronics Engineers.

Wataru Ohnishi (Member) received the B.E., M.S., and Ph.D. degrees from the University of Tokyo, Japan in 2013, 2015, and 2018, respectively. Presently, he is a research associate with the Department of Electrical Engineering and Information Systems, Graduate School of Engineering, the University of Tokyo. His research interest includes high-precision motion control. He is a member of the Institute of Electrical and Electronics Engineers.

Hiroshi Fujimoto (Senior Member) received the Ph.D. degree in the Department of Electrical Engineering from the University of Tokyo in 2001. In 2001, he joined the Department of Electrical Engineering, Nagaoka University of Technology, Niigata, Japan, as a research associate. From 2002 to 2003, he was a visiting scholar in the School of Mechanical Engineering, Purdue University, U.S.A. In 2004, he joined the Department of Electrical and Computer Engineering, Yokohama National University, Yokohama, Japan, as a lecturer and he became an associate professor in 2005. He has been an Associate Professor of the University of Tokyo since 2010. He received the Best Paper Awards from the IEEE Transactions on Industrial Electronics in 2001 and 2013, Isao Takahashi Power Electronics Award in 2010, Best Author Prize of SICE in 2010, the Nagamori Grand Award in 2016, and First Prize Paper Award IEEE Transactions on Power Electronics in 2016. His interests are in control engineering, motion control, nano-scale servo systems, electric vehicle control, motor drive, visual servoing, and wireless motors. He is a senior member of IEE of Japan and IEEE. He is also a member of the Society of Instrument and Control Engineers, the Robotics Society of Japan, and the Society of Automotive Engineers of Japan. He is an associate editor of the IEEE/ASME Transactions on Mechatronics from 2010 to 2014, the IEEE Industrial Electronics Magazine from 2006, the IEE of Japan Transactions on Industrial Application from 2013, and the Transactions on SICE from 2013 to 2016. He is a chairperson of the JSAE vehicle electrification committee from 2014 and a past chairperson of the IEEE/IES Technical Committee on Motion Control from 2012 to 2013.

Yoichi Hori (Fellow) received the B.S., M.S., and Ph.D. degrees in electrical engineering from the University of Tokyo, Tokyo, Japan, in 1978, 1980, and 1983, respectively. In 1983, he joined the Department of Electrical Engineering, the University of Tokyo, as a Research Associate. He later became an Assistant Professor, an Associate Professor, and, in 2000, a Professor at the same university. In 2002, he transitioned to the Institute of Industrial Science as a Professor in the Information and System Division, and in 2008, to the Department of Advanced Energy, Graduate School of Frontier Sciences, the University of Tokyo. From 1991 to 1992, he was a visiting researcher at the University of California at Berkeley. His research fields are control theory and its industrial applications to motion control, mechatronics, robotics, electric vehicles, and wireless power transfer. He has been the Treasurer of the IEEE Japan Council and Tokyo Section since 2001. He was the winner of the Best Transactions Paper Award from the IEEE Transactions on Industrial Electronics in 1993 and 2001, of the 2000 Best Transactions Paper Award from the Institute of Electrical Engineers of Japan (IEEJ), and of the 2011 Achievement Award of the IEEJ. He is an AdCom member of the IEEE Industrial Electronics Society. He is also a member of the Society of Instrument and Control Engineers, Robotics Society of Japan, Japan Society of Mechanical Engineers, and the Society of Automotive Engineers of Japan. He is the past president of the Industry Applications Society of the IEEJ, the president of the Capacitors Forum, the chairman of the Motor Technology Symposium of the Japan Management Association, and the director of Technological Development of the Society of Automotive Engineers of Japan.